Variation of wettability across different lithotypes in a reservoir and its impact on Digital Rock Physics pore scale simulations.

Titly Farhana Faisal[1], *Franck Nono*[1], *Mohamed Regaieg*[1], *Regis Brugidou*[1], *Florent Fischer*[1] and *Cyril Caubit*[1]

[1]TotalEnergies, CSTJF, Avenue Larribau, 64000 Pau, France

Abstract. Digital Rock Physics (DRP) technology offers a faster and cost-effective approach to obtain simulated relative permeability curves that can provide reservoir engineers with additional petrophysical inputs for their simulations.

Recent works of Regaieg et al. 2023 [1] have demonstrated the impact of using large pore network simulations coupled with fast, and practical, pore-scale wettability characterization for enhancing the predictive power of DRP simulations to compute relative permeability curves. Although fast, this wettability experiment is still the bottleneck of DRP simulations workflow as it takes around three-four months whereas the imaging and numerical simulations take around two weeks. Therefore, understanding the variability of wettability across a reservoir is crucial to assess how often the wettability anchoring experiment is needed to estimate relative permeability across the reservoir. In this work, we have applied the same DRP workflow on two reservoir sandstones (representing two different lithotypes of rocks) from the same well in an operational context. Pore-scale wettability characterization (such as the fraction of oil/water-wet pores, correlation of wettability to pore-size etc.) and anchoring information (for e.g., estimation of remaining oil saturation, capillary-end effect, measurement of permeabilities at end-points) obtained from both samples revealed two distinct models of mixed-wet type of wettability: MWS (Mixed-wet Small) & MWL (Mixed-wet Large). Using the relevant range of parameters for each wettability type, we performed experimental design studies to run thousands of flow simulations on very large pore network models for both samples. Results show the subsequent impact on flow simulation results and reinforce the importance of fast wettability characterization for DRP simulations, especially when the assumption of similar wettability cannot be justified across the well or reservoir due to lack of prior knowledge or experience.

1 Introduction

To meet the growing demand for energy in a fair and responsible manner, oil and gas production must be fast and efficient in terms of costs and emissions. In this context, accelerating petrophysical synthesis via digital approach that relies less on extensive SCAL experiments, can play a vital role in rapid appraisal and development of oil fields. Digital Rock Physics (DRP) offers such a cost-effective and efficient approach to computing relative permeability curves for rock/fluid systems. While the potential of DRP has been recognized for well over two decades, truly predictive yet industrially practical solutions have been elusive until recently [1,2]. These recent works of Regaieg et al. have demonstrated the predictive power of DRP to obtain relative permeability by combining large simulations with innovative wettability anchoring experiment for a mixed-wet (MW) Bentheimer formation [1] as well as for a Reservoir Sandstone [2].

It is well known that wettability strongly affects relative permeability [3]. It plays a pivotal role in modelling of multiphase flow as it governs capillary forces and order of invasion. Indeed, accurate characterization of wettability has been identified [4-7] as one of the most complex and important steps for reliable prediction of multiphase properties using simulations. Traditional wettability tests, such as the Amott-Harvey tests are time-consuming and resulting qualitative description of wettability such as water-wet, oil-wet, or mixed-wet often lack the necessary detailed pore-scale insight required for accurate simulations. The situation is even more complex for mixed-wet wettability [8], which is the case for most oil reservoirs. A higher number of uncertain parameters remain, especially for mixed-wet cases as the contact angles, the fractions of OW (oil-wet) and WW (water-wet) pores, wettability spatial correlation and wettability radii correlations are all important parameters that could impact the simulation results. Simulation studies [9,10] that have used wettability distributions obtained from in-situ Micro-CT experiments [11,12], have shown that random allocation of contact angle distributions and random spatial wettability

* Corresponding author: titly.farhana-faisal@totalenergies.com

assumptions lead to poorer predictions of relative permeability, particularly for mixed-wet media.

Indeed in-situ contact angle measurements using X-ray micro-CT has gained traction in recent years. However, these measurements are dependent on three-phase contact line region (that are sensitive to image resolution and segmentation pixelation) and involve manual [13] or intensive image processing [12,14] that are unsuitable for industrial applications. Insufficient resolution can lead to contact angle values close to 90 degrees, accompanied by large standard deviations [15]. Moreover, contact line pinning effects are included in automated contact angle measurements which are different from the advancing/receding contact angles needed in PNM simulator. To circumvent these challenges, an innovative DRP simulation anchoring experiment was developed [1] for a rapid and straightforward implementation within an industrial workflow. In fact, contact angles are not directly measured from image analysis in our approach. Instead, indicative ranges of advancing contact angle values are obtained from the observed volumes of imbibed oil/water during spontaneous displacement steps, and the presence of capillary end-effect in the sample. Additionally, for mixed-wet systems, visual screening of the pore occupancies during the Amott-like DRP wettability experiment also allows us to assess other parameters like fraction of OW/WW pores, type of MW model and spatial correlation lengths where applicable as shown previously in [1].

Despite the solid starting point for simulations using the parameters described above, there remains a significant uncertainty in these inputs. This is why we also developed a statistical uncertainty workflow [16] that varies the uncertain pore network simulation parameters to run thousands of simulations. This exposes the resulting dispersion in simulated relative permeability curves, which we then constrain using fast measurements (of permeabilities and saturations at end-points) made during the anchoring experiment. This approach has led to predictive DRP Kr results that we have validated previously with SCAL measurements [1,2]. However, while it is interesting and faster than traditional Amott measurements, it is still a bottleneck in the current DRP workflow as it adds three-four months to a simulation workflow that could otherwise be completed in two/three weeks. Assessing how often the wettability experiment is needed, and its impact on reliability of DRP relative permeability simulations, is therefore crucial as it can significantly increase the number of rock type characterizations during field development (especially when same wettability can be assumed across different facies).

A first case of such extrapolation has been demonstrated in [2], where one wettability experiment was performed, and assuming the same wettability for other facies in the reservoir, new relative permeability simulations were conducted for another rock facies in two weeks. Comparison to SCAL validated these results and provided more confidence. However, the wettability type in [2] was fractional-wet (i.e. contact angles are not correlated to the size of the pores) and porosity-permeability of the two rocks studied were very close. Therefore, more tests were recommended especially for cases where wettability is correlated to pore size.

To investigate this further, we have applied the same DRP workflow on three reservoir sandstones (representing different lithotypes LT1, LT2 & LT3, and bigger permeability range) from the same well in an operational context. The study was set up as follows:

(1) DRP wettability anchoring experiment was performed on high permeability rock sample (LT1). Mixed-wet Small (MWS) type wettability was found, and relative permeability simulations were run for the relevant range of parameters.

(2) A second rock sample (LT2) with similar high permeability, mineralogy and pore size distribution was used to test the same wettability assumption found in LT1. Results were compared with available SCAL measurement on a sister sample.

(3) Another DRP wettability anchoring experiment was performed on tighter rock sample (LT3). Mixed-wet Large (MWL) type wettability was found, and relative permeability simulations were run for the relevant range of parameters.

(4) Wettabilities and networks were then used interchangeably to assess the impact on Kr simulations due to assumed vs. measured wettability, thus extending our study to a case where wettability is correlated to pore radii.

2 Materials and methods

2.1. Samples

In this work, we have used three reservoir sandstones from the same well. In terms of sedimentary facies, both are characterized as massive fine to medium high density turbiditic sand. All three rocks have similar minerology, composed primarily of quartz (88 – 93%). Further lithology classification separates them into three lithotypes that we will refer to as LT1, LT2 and LT3. Where, LT1= clean tectosilicates (permeability range greater than 1000mD), LT2=clean tectosilicates (permeability range around 100 mD - 1000mD) and LT3 = tectosilicates with slightly shaly texture (permeability range in few hundreds of mD). Sample dimensions and petrophysical properties are shown in Table 1. Cross section image of the 10mm diameter mini-plugs at 5.3 µm pixel resolution acquired using Zeiss Versa 520 microtomograph are shown in Figure 1. The permeabilities shown are measured physically, and the porosities have been determined through image processing using differential imaging [17] for LT1 and LT3. Amount of sub-resolved porosities are also

indicated, showing that higher percentage of unresolved pore in LT3 at the same imaging resolution. For idea on representativity, we can also note the porosities (Φ_{total_HE}) for samples from same depth and lithotype evaluated at the plug (diameter = 38 mm) scale using Helium porosimeter. Φ_{total_HE}: for LT1= 24 %, LT2=19.4 %, LT3=17.6%.

Table 1. Sample properties.

Sample	D (mm)	L (mm)	K_w (mD)	Φ_{total} (%)	Φ_{sub} (%)
Reservoir rock LT1	10	15	4650 +/- 400	21.9	~ 3.8
Reservoir rock LT2	10	16	1813 +/- 200	19.5	N/A
Reservoir rock LT3	10	17	165 +/- 10	19.7	~ 8.1

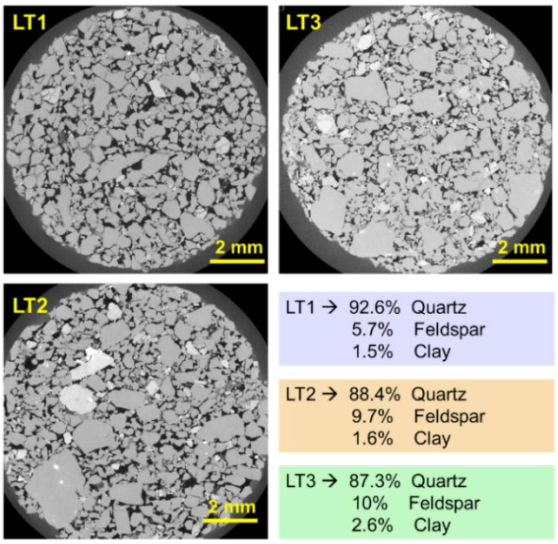

Fig. 1. Cross section image of the 10mm diameter mini-plugs (left) LT1 and (right) LT2 at 5.3µm pixel resolution acquired using Zeiss Versa 520 microtomograph. Average pore sizes of LT3 are visibly smaller than LT1.

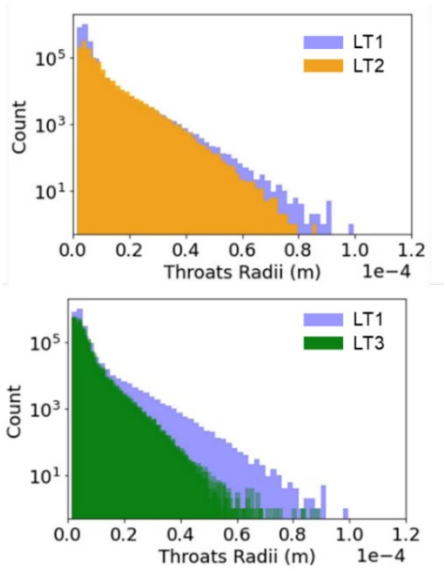

Fig. 2. Comparison of pore throat size distribution obtained from pore network models of LT1, LT2 and LT3

Pore throat size distributions obtained from extracted pore network models confirm the smaller pore sizes seen in LT3 image (Figure 2). These information show that LT2 and LT1 are closer in permeability and pore size distribution compared to LT3, justifying selection of LT2 as a first candidate for testing the same wettability assumption as LT1.

2.2. Enhanced Super Resolution images and large-volume pore network extraction

A typical DRP simulation workflow begins with micro-CT image acquisition of rocks. Acquired images are then segmented to differentiate the rock from the pore space. The identified pore space is finally used to perform flow simulations to calculate advanced rock properties like relative permeability and capillary pressure. Research [18, 19] shows that well-characterized pore space geometry leads to good performance of flow simulators. However, as with all imaging based workflows, there is an inherent trade-off between acquisition speed, scanned volume size, and obtained resolution. Higher resolution limits field of view and vice-versa, impacting the representativity of rock sample volumes used in simulations.

In an effort to bypass this compromise, we have implemented Enhanced Super Resolution Generative Adver-sarial Network (ESRGAN) method [20] with some adjustment to adapt it to micro-CT images (more details in [20]). The approach includes a training and inference step. We have made the training parallel using multiple nodes and multiple GPUs in each node. The training is performed using two scans (at low and high resolution) of the same spatially registered volume. 2500 crops of 384*384 pixels images are made to form the training dataset. Upon completion, the trained model is applied on a large-volume low resolution image to enhance the image resolution by a factor of 4. Low resolution values= 10.6µm, 10.6µm and 12µm for LT1, LT2 & LT3 respectively. Resolution after enhancement= 2.65 µm, 2.65 µm and 3 µm for LT1, LT2 & LT3 respectively. Generated super-resolved images were of approximately 3300x3300x3300 voxel in size.

Figure 3 showcases the results obtained through Factor 4 resolution enhancement, demonstrating high perceptual quality that effectively captures intricate rock textures and previously unresolved clay features in the low-resolution image. We have previously assessed the quality of such super-resolved images by comparing petrophysical metrics for rock images [2, 21].

To segment the super resolved images, we utilized the 2D Trainable WEKA Segmentation method [22], which employs the Random Forest (RF) machine learning algorithm. Previous research [23] shows that with experienced training, Trainable WEKA Segmentation outperformed seven other image-processing pipelines without the need for prior filtering. Benchmark study conducted by Reinhardt et al [24] further reveals that RF-based approaches benefit from lower user bias compared to other machine learning and conventional segmentation

techniques, thanks to continuous interaction between experienced users and the RF classifier.

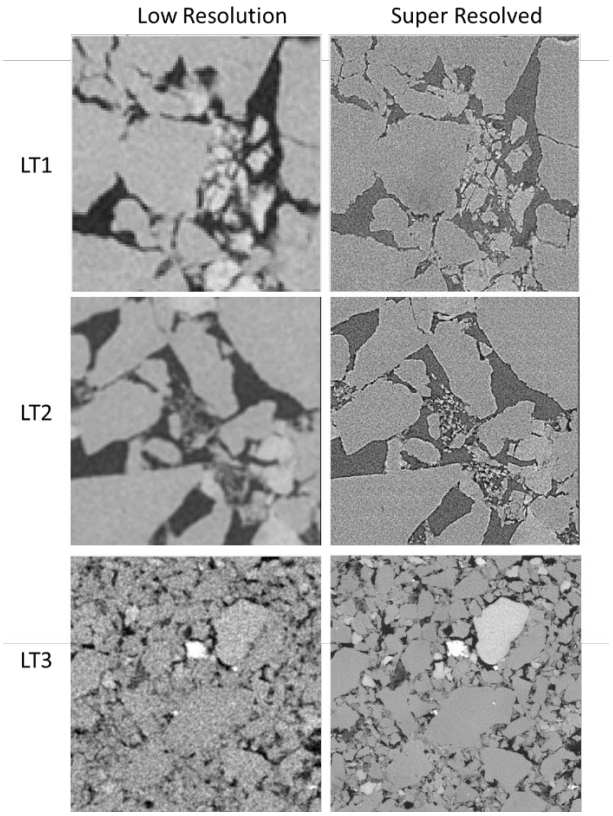

Fig. 3. Comparison between low resolution and super resolution cropped images of reservoir rocks. Images have been enhanced by a resolution factor of four. Low resolution values: 10.6µm, 10.6µm and 12µm for LT1, LT2 & LT3 respectively. Resolution after enhancement: 2.65 µm, 2.65 µm and 3 µm for LT1, LT2 & LT3 respectively

Pore network models do not conduct flow simulations directly on the segmented images. An extraction step simplifies the 3D image to represent geometric and topoligal information of the underlying pore skeleton. Such large images generated from super resolution need efficient treatment to avoid memory limitations. This has been managed by using an in-house stitching algorithm [21]. For the individual extractions, we utilized a pore network extraction platform called GNextract, developed in collaboration with Imperial College London [25], and built a larger network by combining overlapping sub-volumes of extracted networks. With this methodology, we extracted one pore network each for LT1 (Φ_{SR}=20.8%, K_{abs}=3.6 D) and LT2 (Φ_{SR}=18.8%, K_{abs}= 2.3 D), and, five pore networks for LT3 to account for slightly greater heterogeneity observed in the sample (Φ_{SR}= 14.5 - 15%, K_{abs}= 110 – 225 mD), where Φ_{SR} is porosity of super-resolved images and K_{abs} is simulated absolute permeability. LT1 and LT2 networks had around 1.5 million elements each, representing a physical volume ≈ 8.5 mm^3. Each LT3 network had on average 2.4 million elements and represented a physical volume ≈ 4.8 mm^3.

2.3. Wettability anchoring experiment

As discussed earlier, wettability characterization plays key role in making pore network modeling simulations more predictive, and we have developed a fast DRP wettability experiment to better characterize wettability at pore scale. At its core, the experiment is basically a series of spontaneous and forced displacement cycles using relevant fluid pairs similar to the known SCAL Amott wettability experiment. The key distinction is the utilization of Micro-CT images to capture the different displacement steps, which allows direct visual investigation at the pore-scale.

In this study, an upgraded version of the previous wettability anchoring experiment protocol (described in details in [1,2]) has been followed for both LT1 and LT3 samples. The upgrade considers the recommendations highlighted by the experimental investigations from our SCAL laboratory [26]. The main motivation for the upgrade is to avoid dopants in formation brine during ageing process with dead oil (DO) as dopants can impact the wettability alteration process. Details of the upgraded experiment have been described in submitted manuscript SCA2024-1025 [27].

Two wettability experiments were performed in this study: one for sample LT1 and another for sample LT3. The same fluids (brine composition, dead oil, and mineral oil) have been used in both experiments. We used reservoir dead oil (DO) for the aging processes and mineral oil (Marcol 52) for displacement steps. The experiment commences by mounting the sample into a flow cell under a net confining stress of 90 Bars. The initial step involves achieving the initial water saturation (Swi) viscous displacement with M52 and highly doped brine. Image acquired at this step is used for assessment of the Swi saturation distribution. Next, instead of ageing the sample like in the previous workflow, the plug is cleaned again and full saturated with formation brine without any dopant. This is the key additional step that is introduced in the upgraded wettability experiment. Permeability measurement is re-checked and primary drainage is re-performed by viscous flooding using M52 by ensuring the same flow parameters as the previous primary drainage (flowrates, gradient pressures). At the end of this step, we check that we obtain similar $K_o(S_{wi})$ as before. Another image at this step is useless as no contrast can be observed between brine and oil. It is assumed that for similar $K_o(S_{wi})$, flowrates and gradient pressures, same pore occupancies are obtained for the two Swi establishment steps (with and without dopant in brine).

The mineral oil is then replaced with toluene and subsequently with dead oil at 90°C. Afterwards, the sample is left to age for 1 month at 90°C, during which a total of 10 pore volumes (with a change of injection direction after 5 pore volumes) was injected to avoid any gradient on wettability distribution. At the end of the ageing process, $K_{ro}(S_{wi})$ with dead oil is measured, the

temperature is decreased to 60°C and only 1 pore volume of toluene is injected to replace dead oil without impacting the actual plug's wettability. It is followed with the injection of at least 6 pore volumes of M52 to replace toluene and the decrease of temperature till ambient temperature.

Once the temperature is reduced and the replacement is completed, spontaneous imbibition phase is initiated using a one-end-opened protocol. To be able to visually track saturations, a lightly doped formation brine is introduced to the sample for all subsequent steps as it no longer impacts the already altered wettability. Saturation changes are tracked via image processing in both the resolved and unresolved part of the porosity using approach described in [28]. During spontaneous imbibition, water spontaneously infiltrates the sample from the bottom face while oil is expelled from the same side, establishing a counter-current imbibition phenomenon. To ensure controlled conditions and a continuous contact between water and the bottom face of the rock, we use a water leaching process with an extremely low capillary number ($8x10^{-9}$) to remove the generated oil from the diffuser without inducing forced water flow into the sample.

After the spontaneous imbibition, a forced imbibition at very low capillary number (1E-08) to visualize and quantify saturation profiles on the capillary end-effect (zone of zero capillary pressure) is performed. Finally, forced imbibition is continued at a high capillary number (1E-05) to approach the residual oil saturation. At the conclusion of each phase of the experiment, micro-CT acquisitions are conducted to capture detailed imaging data. This enables us to have valuable information about the fluid distribution within the sample at different stages of the experiment.

2.4. Wettability experiment interpretation for simulation inputs

Images acquired during the wettbaility experiment are processed to obtain saturation profiles. Images before and after the two-weeks long spontaneous imbibition show (Figure 4) that water imbibed in both LT1 and LT3 experiments, but the pore sizes invaded were different in each case (visible in Figure 4 zoomed section and illustrated more quantitatively later in section 2.4).

Water saturation increased from 15% at Swi to 65% during spontaneous imbibition for LT1 sample. In comparison, lower water saturation increase was noted in LT3, where the water primarily went into smaller pores and saturation increased from 20% at Swi to 40% during spontanous imbibition. As water can only imbibe through the connected water-wet pores, and that wettability of pores where trapping occurs would be unknown, it is worth noting that volumes computed essentially provide the minimum fraction of pores that is WW. Furthermore, the low flow-rate forced imbibition step allows us to observe any capillary-end effect at the sample outlet.

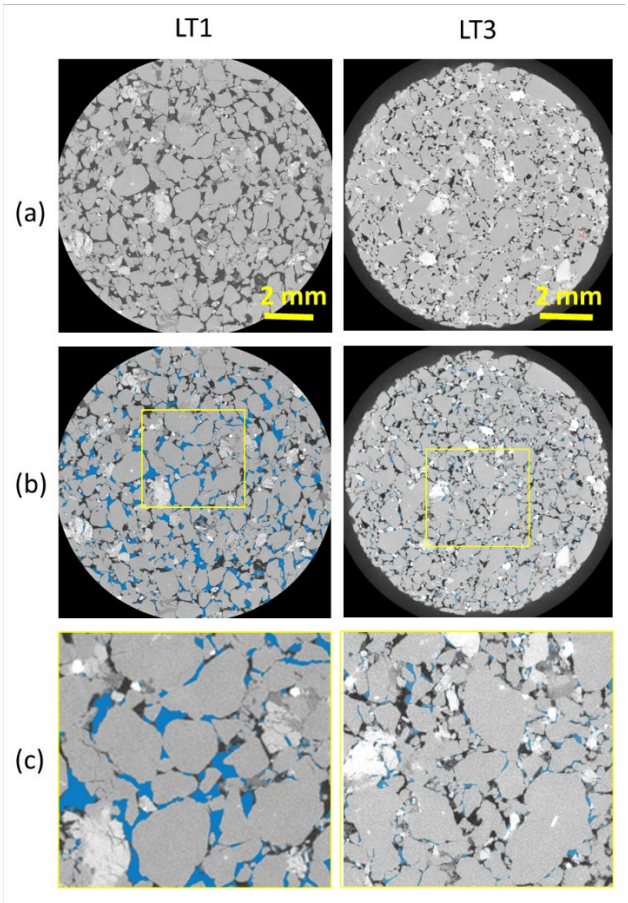

Fig. 4. Images showing saturation states before and after spontaneous imbibition in LT1 and LT3.

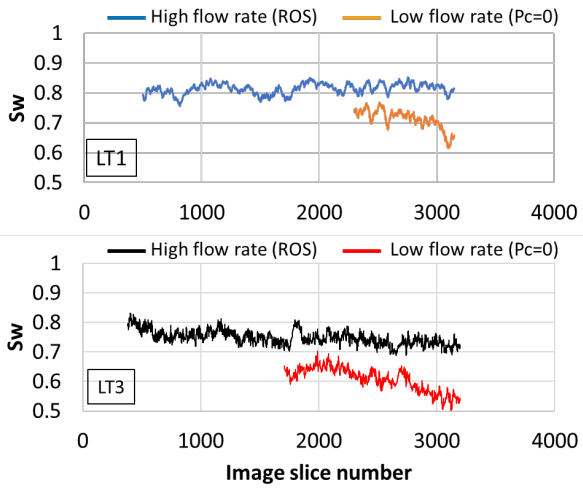

Fig. 5. Water saturation profiles for forced imbibition low- and high- flow rates. The low-flow rate investigation is only interesting at the sample outlet, to observe capillary end-effect presence, hence only partial image of the sample is acquired for this step. The high-flow rate shows remaining oil saturation (ROS) profile for the full length of the sample.

Both samples display a degree of capillary end-effect to oil (Sw profiles shown for low flow rate forced

imbibition in Figure 5), indicating presence of OW part in the pore network. In addition to the volumes of water imbibed during the spontaneous imbibition steps, the saturation of oil at the outlet (where Pc=0) further helps us characterize the oil-wet fraction in the system. Both these observations help us draw a range for the suitable fraction of WW/OW pores for the network simulations. In reality however, there are some uncertainties that need to be taken into consideration: 1) due to imaging artefacts, some end-slices needed to eliminated from the tomographs during saturation quantification and 2) as the samples used in this study were semi-unconsolidated in nature, the sample radius close to the outlet was uneven, leading to additional uncertainty related to the outlet location. Extrapolated values for Sw@Pc=0 are therefore noted as 60% for LT1 and 50% for LT3. An uncertainty bracket (of +/- 10%) is added to take this into consideration. The Sw@Pc=0 are then used as a rough selection criteria for fast PNM simulation sensitivity studies on the respective networks to find out the range of suitable OW/WW fractions that are needed to achieve this. Final range for fraction of WW pores used in the simulations for the LT1 and LT3 networks are shown in Table 2.

Although there is an oil-wet part in the sample, save a few odd pores, virtually no oil imbibition was observed during the two-weeks long spontaneous drainage for both samples. As the analysis does not directly provide contact angles values, the observed capillary end effect indicating oil wetness and the virtually undetectable oil imbibition during spontaneous drainage suggest that a considerable number of the oil-wet pores have receding contact angles below 90°. Or that stronger OW pores if present, are few and predominantly disconnected. Thus, we selected medium to low oil-wet contact angle values to represent the mean for normal distribution used in the simulations. Standard deviation to the mean provides tail values that can account for few strongly OW pores.

Figure 5 also shows the Sw profile at remaining oil saturation (ROS). Given the significant fractions of water-wet parts detected in both LT1 and LT3, the lower ROS values are another indication of the sample's mixed wettability. Additionally, these experiments also provided end point measurements. Based on the uncertainties related to Sw quantification and measured permeabilities, envelopes are used for the simulation's selection process.

- LT1: 0.3 < Krw @ ROS < 0.6
- LT1: 0.15 < Sor < 0.21
- LT3: 0.25 < Krw @ ROS < 0.5
- LT3: 0.16 < Sor < 0.3

As both samples exhibited mixed wet pores, it was important to identify the wettability model type: Some authors [29] proposed 3 models: Fractional-wet, Mixed-wet small and mixed-wet large models. Figure 4 shows water-wet (WW) pores in blue for both LT1 and LT3 samples. We recall that oil that imbibes into the system in spontaneous drainage does not have access to the full rock as a part of the porosity is already filled with oil. Therefore, we propose to perform this analysis on the water-wet pores that had access to all the pore space during the spontaneous imbibition. Figure 6 shows the volumetric fraction of water-wet pores as a function of the pore radii. The plots clearly reveal two distinct models of mixed-wet type of wettability: MWS (Mixed-wet Small) for LT1 & MWL (Mixed-wet Large) for LT3.

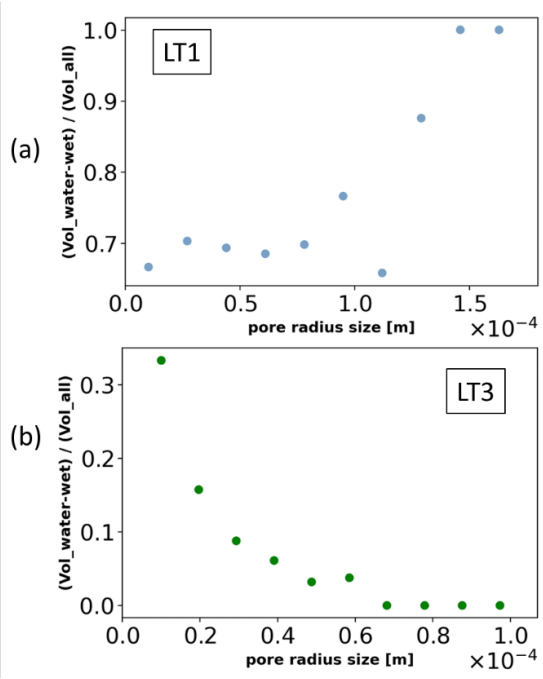

Fig. 6. The water-wet volumetric fraction as a function of the pore radius showing correlation of wettability with pore size.

2.5. Pore Network Simulation and statistical workflow

Using the extracted pore networks and relevant wettability inputs, we proceeded to conduct two-phase flow simulations for all three rock networks. For simulations, we used DynaPNM, which is TotalEnergies' proprietary multiphase pore network simulator, as described in reference [30]. The simulator is used in quasi-static mode as all the cases that we study in this paper are capillary dominated.

Initially, the pore network is filled with water. Next, a primary drainage process is simulated to establish the target initial water saturation (Swi). Since the network is assumed to be water-wet, oil injection follows an invasion percolation regime. Low Swi values can be achieved because water can escape through the wetting layers.

After primary drainage, a waterflood occurs following an aging process that changes the wettability of oil-filled pores. The fraction of these oil-filled pores in the network, along with a range of contact angle values, are crucial inputs for the simulation at this stage. During waterflood, water spontaneously fills the water-wet portion of the network through piston-like displacement and snap-off mechanisms. Smaller pores are filled first, followed by larger ones. The defending oil phase escapes through oil-filled pores. Finally, negative capillary

pressure is applied to initiate filling of the largest pore elements, allowing oil to escape through the outlet via the center of oil-filled pores or oil films. The simulation continues until all the oil is trapped within the network.

The simulator has been parallelized enabling the simulation on large networks comprising tens of millions within a few hours as described in [22].

Although we conducted a wettability anchoring experiment, there is still considerable uncertainty in the input parameters. To tackle this issue, we designed a statistical uncertainty workflow to integrate this information. In this workflow, we varied the uncertain parameters of the pore network simulation based on the ranges determined from the anchoring experiment.

Table 2. Simulation parameters used to account for wettability interpretations of LT1 and LT3.

	Value/ Range LT1	**Value/ Range LT3**
PD receding contact angle distribution	Normal distribution	Normal distribution
PD receding contact angle standard deviation	4°-8°	4°-8°
Mean receding PD distribution	20°-30°	20°-30°
WF dist1 (oil-wet) advancing contact angle distribution	Normal distribution	Normal distribution
WF dist1 (oil-wet), advancing contact angle standard deviation	4°-8°	4°-8°
Mean advancing WF dist1 (oil-wet) contact angle	100°-120°	110°-120°
WF dist 2 (water-wet) advancing contact angle distribution	Normal distribution	Normal distribution
WF dist2 (water-wet), advancing contact angle standard deviation	5°- 10°	4°- 8°
Mean advancing WF dist2 (water-wet) contact angle	70°-89°	70°-89°
Fraction of distribution 2 (water-wet fraction)	0.5-0.65	0.2-0.5
Spatial correlation length	4 - 20	4 - 6
Wettability model	Mixed-Wet Small	Mixed-Wet Large
Initial water saturation	0.15	0.2

Simulation parameters used to account for wettability interpretations of LT1 and LT3 are specified in Table 2. With these parameters, we generated thousands of input files for DynaPNM simulations using the WSP method [31]. Approximately 1500 realizations were created for each simulation study. These generated files were then used to run flow simulations on TotalEnergies' supercomputer. A selection process was performed to retain only those realizations that aligned with the observed ROS and Krw@ROS obtained from the wettability anchoring experiment.

Following the selection exercise, a simulation ranking procedure was implemented based on the oil production achieved after a specified amount of water injection corresponding to each relative permeability curve. This ranking process allowed us to define three scenarios:

- P10: an optimistic scenario in which only 10% of the simulations produce more than this case
- P50: a median scenario in which 50% of simulations produce more than this case
- P90: a pessimistic scenario in which 90% of the simulations produce more than this case

Generated DRP relative permeability curves were Corey fitted to facilitate their use in Reservoir simulations.

3 Analysis of simulation results

A summary of the simulations performed for this study are shown in the below simulation matrix:

Table 3. Simulation matrix showing the combination of wettability inputs and pore networks used to perform five simulation studies

	Wettability interpretation LT1	Wettability interpretation LT3
Pore Network LT1	✓	✓
Pore Network LT2	✓	
Pore Network LT3	✓	✓

As LT1 and LT2 were found to be closer in terms of permeability and pore size distribution, it was selected as a first candidate for testing the same wettability assumption. Thus, MWS wettability derived from LT1 experiment was used to perform simulations in LT2 network. Then, the same MWS wettability was also used for LT3 network. However, due to the tighter permeability and smaller pore sizes seen in LT3, we evaluated its wettability separately. Simulations on LT3 were therefore repeated with MWL wettability derived from the LT3 experiment, to assess possible impact of assumed vs. measured wettability in a scenario where wettability is correlated to pore size. Lastly, the MWL wettability was also tested on LT1 network.

Figures 7-9 show our simulated results after the selection exercise that keeps realizations in accordance with the observed end-points during the wettability experiments. The ranked P10 (green), P50 (orange), and P90 (red) curves are highlighted.

Simulation results for LT1 network using the MWS wettability derived from its wettability anchoring experiment are shown in Figure 7. The same MWS wettability assumption was used for LT2, and results compared with SCAL experiment available on a sister sample are shown in Figure 8. The SCAL experiment was performed on a large sister sample of LT2 core of 5 cm

diameter and 20 cm length. This full -size core had a porosity of 20% with an absolute brine permeability of 2198 mD. Swi of 0.148 was achieved via primary drainage with viscous oil. The same dead oil was used in the SCAL and DRP wettability experiment performed on LT1. However, due to plugging issues faced during the ageing of the plug, the coreflooding steps were completed with mineral oil Isopar that was able to reproduce the correct viscosity ratio. Imbibition process was run at multi-rate constant injection flowrates and 1D core analysis software called CYDAR® was used to perform history match on experimentally monitored parameters like pressure gradient, oil production vs. time data and saturation profiles obtained through 2D X-ray imaging. Numerically interpreted Kr curves were subsequently obtained by inverse analysis. To account for uncertainties in the inversion of experimental data, the SCAL data is represented by multiple realizations (where we considered uncertainty ranges for measured production data and pressure gradients. The same saturation profiles were used for the different realizations). Both the DRP simulated and SCAL Kr curves show Corey fitted results for comparison.

We also analyzed the ratio of relative permeability between the simulations and experiments indicating a strong agreement between the simulated and experimental data We would like to highlight that in unsteady-state relative permeability measurements, the comparison only makes sense after breakthrough (achieved at water saturation of 55%) and before ROS (achieved at water saturation of 83%). In this range of saturations, comparison of DRP Kr water and oil curves with the given SCAL Kr is acceptable while the Kr ratios agreement is excellent. Respective recovery factors (using Buckley Leverett approach) are also shown at the end of this section as well as in Figure 8 (for LT2).

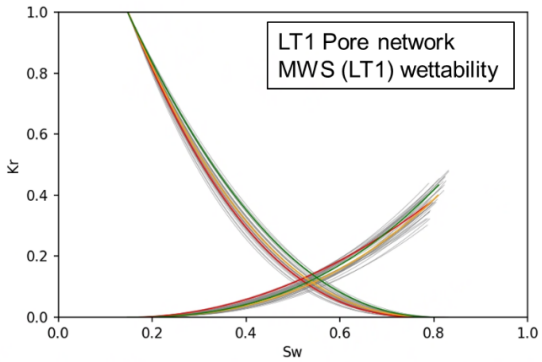

Fig. 7. Selected (grey) and ranked relative permeability curves (at 1PV injected) for LT1 network using LT1 wettability. P10 (Green) represents and optimistic scenario, P50 (orange) represents a median scenario and P90 (red) represents a pessimistic scenario.

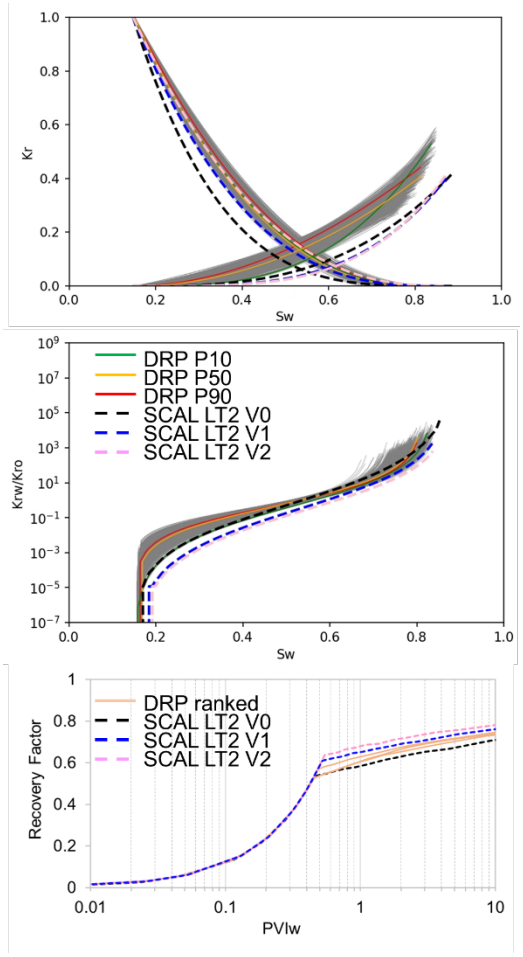

Fig. 8. Selected (grey) and ranked relative permeability curves (at 1PV injected) for LT2 network using LT1 wettability. SCAL Experiment Kr results of sample from type LT2 are compared. P10 (Green) represents and optimistic scenario, P50 (orange) represents a median scenario and P90 (red) represents a pessimistic scenario. Recovery factors for the three DRP ranked curves and the three SCAL realisations are compared.

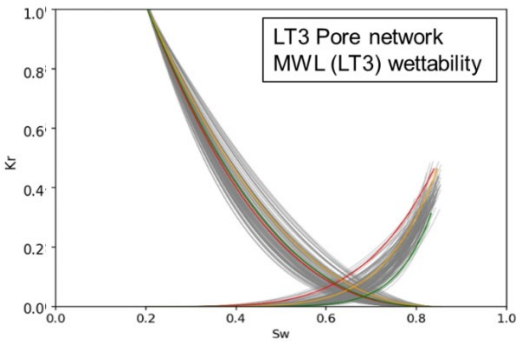

Fig. 9. Selected (grey) and ranked relative permeability curves (at 1PV injected) LT3 network using LT3 wettability. P10 (Green) represents and optimistic scenario, P50 (orange) represents a median scenario and P90 (red) represents a pessimistic scenario.

The similar Kr ratios and RFs for DRP vs. SCAL curves in LT2 gives us more confidence in the predictive capabilities of DRP simulation when same wettability is

assumed for similar topology, mineralogy, and fluids (as observed previously for FW system in [2]). But what about LT3, where permeability and pore size distribution are different? To assess this, we first present LT3 network simulations using its own wettability results in Figure 9.

Next, we look at the impact of measured vs. assumed wettability amongst LT1, LT2 and LT3. Figures 10-15 show comparison of LT1 and LT3 network simulations, when their wettability models were interchanged. In these figures:

For LT1 network:

- Measured wettabillity = MWS & its relevant ranges obtained from LT1 experiment
- Assumed wettability = MWL & its relevant ranges obtained from LT3 experiment

For LT2 network:

- Assumed wettability = MWS & its relevant ranges obtained from LT1 experiment

For LT3 network:

- Measured wettabillity = MWL & its relevant ranges obtained from LT3 experiment
- Assumed wettability = MWS & its relevant ranges obtained from LT1 experiment

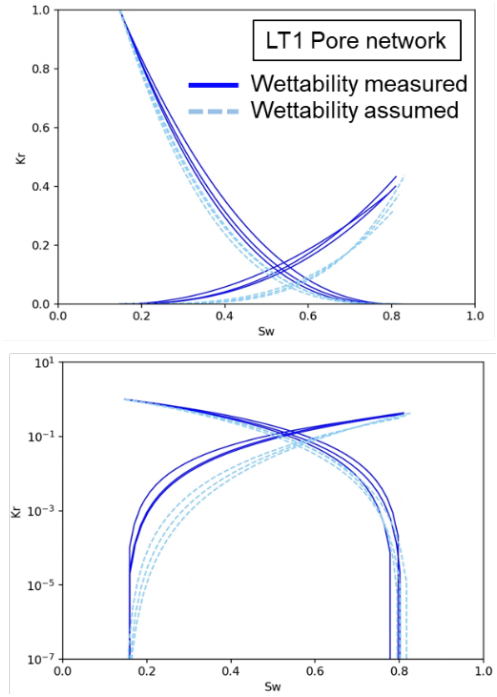

Fig. 10: The ranked Kr curves of LT1 network using assumed and measured wettability.

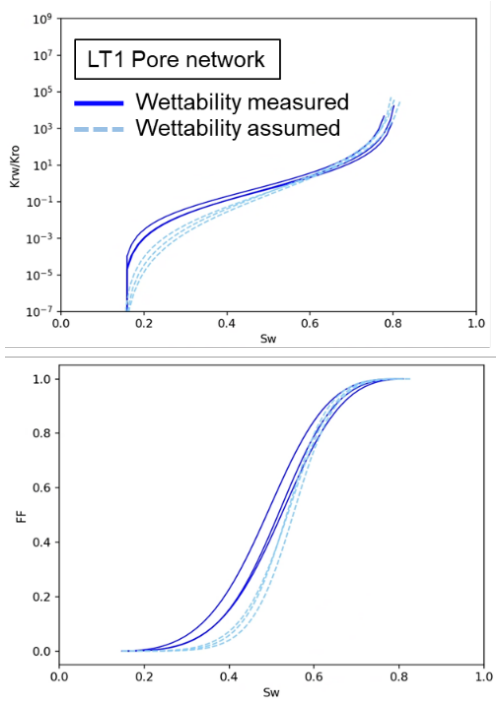

Fig. 11. Krw/Kro ratio and FF for LT1 sample using measured and assumed wettability

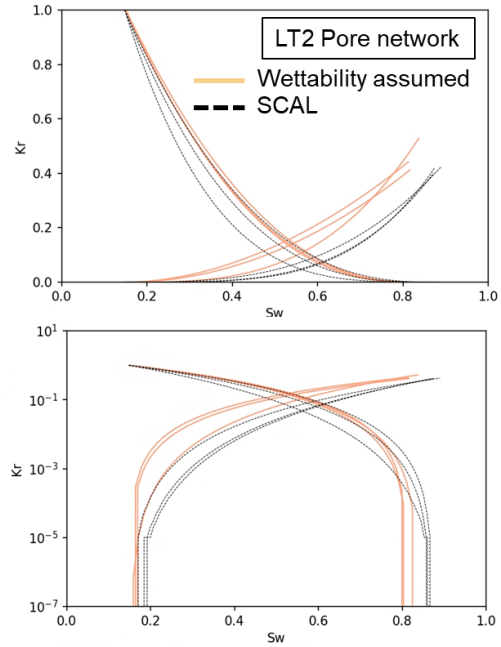

Fig. 12: The three ranked Kr curves of LT2 DRP network using assumed wettability compared to Kr curves obtained from SCAL experiment on another LT2 sample.

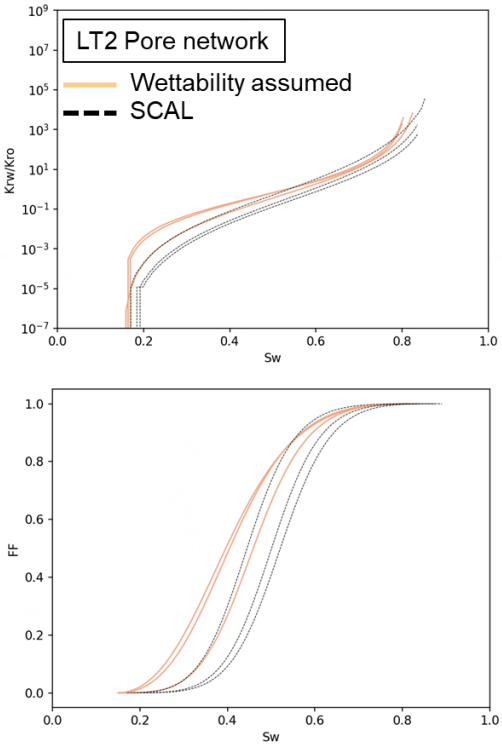

Fig. 13. Krw/Kro ratio and FF for LT2 DRP sample and SCAL experiment compared.

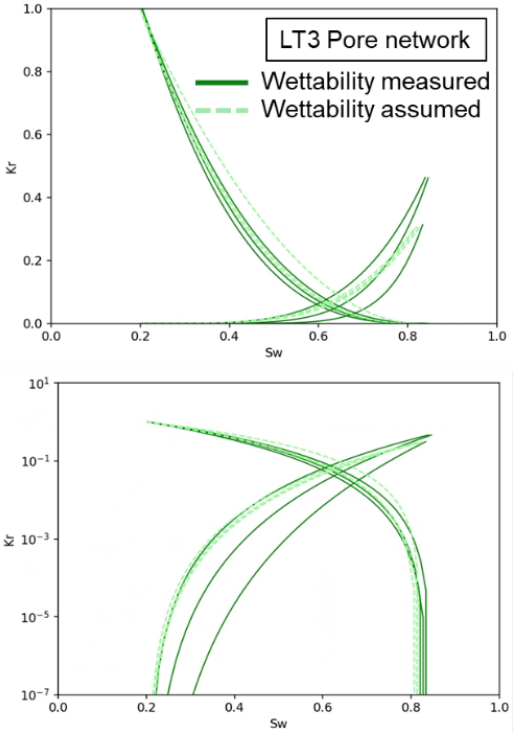

Fig. 14. The ranked Kr curves of LT3 network using assumed and measured wettability.

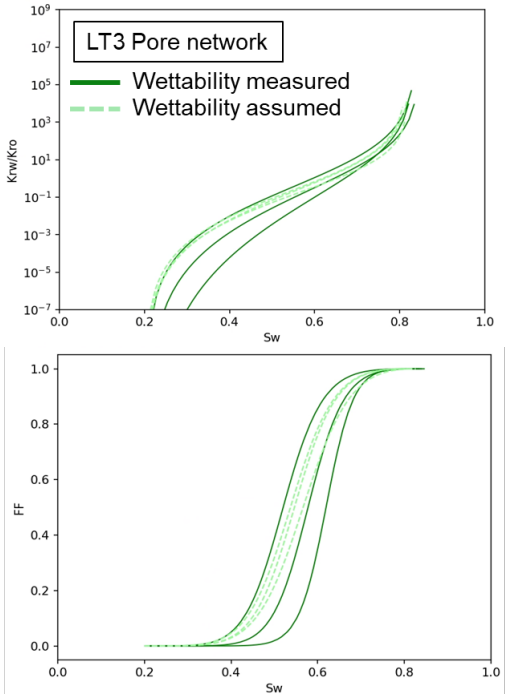

Fig. 15. Krw/Kro ratio and FF for LT3 sample using measured and assumed wettability

To evaluate the recovery factors (RF) associated with the simulated curves, we employed the Buckley Leverett approach. RF for LT1 and LT3 simulation cases are shown in Figure 16. Although we see visible changes in Kr curves shapes, Krw/Kro ratio and FF when wettability model is changed from MWL to MWS and vice-versa (Figures 10 - 15), for this particular case, the recovery factors are not significantly affected. In the bottom-most plot of Figure 16, we compiled the upper/lower RF bounds obtained for both measured/assumed wettability scenario in each case with the RF calculated for the SCAL experiment on LT2. Difference in RF due to network topology change is more noticeable compared to difference due to wettability variation testing for this studied case . We should note that although these results are interesting and help us to extend our understanding to a case where wettability varies with pore radii, more tests are needed before validity of this approach can be generalized. Ideally, factors such as common mineralogy and fluids should also be varied to test the limits of this generalization.

4 Conclusions

In this study, we have furthered our investigation to see if we can potentially accelerate the DRP simulation workflow by reducing number of wettability anchoring experiments, where possible. Within an operational context, three rocks from the same well, but varying lithotypes (LT1, LT2 and LT3) were studied.

Wettability experiments were performed on both LT1 and LT3 samples. One key interesting result of this study is the observation of two different mixed-wet wettability model types (MWS and MWL) for the two samples with

same mineralogy and fluids used during experiments. This shows that topology and pore sizes can have impact on wettability alteration.

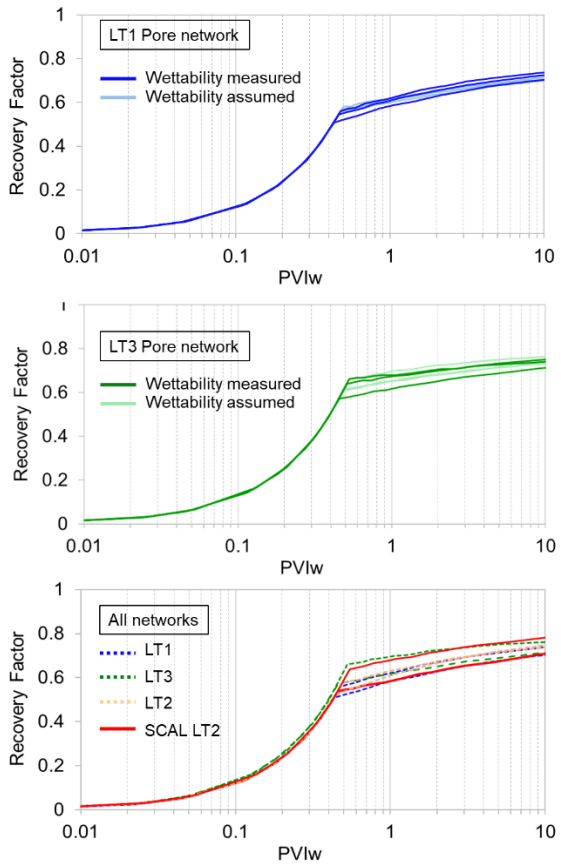

Fig. 16. Recovery Factors plotted against pore volume of water injected. (top) shows RFs computed for all ranked Kr curves contained from DRP simulations on LT1 network using both measured and assumed wettability. (middle) shows RFs computed for all ranked Kr curves contained from DRP simulations on LT3 network using both measured and assumed wettability.(bottom) RFs representing the upper and lower bounds for the simulated and experimental Kr Corey fitted curves are shown.

Wettability experiment results of LT1 were used as inputs to perform DRP Kr simulations on both LT1 and LT2 rocks. LT2 Kr curves were validated by comparing with SCAL experiment results on the same rock type. After successful demonstration of LT1 wettability in LT2, the study was extended to a tighter rock LT3 (with smaller pore size distribution). In parallel, another independent wettability anchoring experiment was performed on LT3 sample to assess the impact of assumed vs. measured wettability on simulation results. Kr simulations were performed on the LT3 pore network using its own wettability as well as that of LT1. Finally, simulations on LT1 network using LT3 wettability were also performed.

Results show that while Kr curve shapes and Kr ratios are visibly affected due to these variations, the recovery factors (RF) evaluated using Buckley Leverett approach were not significantly affected (for the given network topology). The wettability characterizations: MWS for LT1 and MWL for LT3, revealed two distinct and observable wettability models where wettability is correlated to pore size. This extends our previous study [2], where the wettability extrapolation approach was successfully applied to a fractionally wet reservoir sandstone. While these validations provide greater confidence, it is worth recalling that factors which are known to affect wettability alteration such as: mineralogy (primarily quartz), and reservoir fluids (same oil/brine composition) were same for these samples. Therefore, more tests are needed to have better understanding of the domain of validity of the same wettability assumption across different rocks in the same reservoir.

In the future, we could also think of benefitting from such simulation sensitivity analysis for cases where one wettability experiment has been performed and other samples from the same reservoir are in consideration for further DRP analysis. Given same mineralogy and fluids, we could then vary the wettability parameters for different networks across the reservoir and assess the impact on Krs and recovery factors. Such sensitivity studies could provide valuable recommendations on when a new wettability experiment is needed.

Acknowledgements

The authors would like to thank TotalEnergies management for the authorization to publish this work. We also thank the Recovery Mechanism Characterization (RMC) Laboratory at TotalEnegies, Pau, France for the LT2 SCAL Kr experimental data.

References

1. Regaieg M., Nono F., Farhana Faisal, T., Rivenq R. Large Pore Network simulations coupled with innovative wettability anchoring experiment to predict relative permeability of a mixed-wet rock. Transport in Porous Media, 147, 495–517 (2023).
2. Regaieg M., Farhana Faisal, T., Nono F., Pairoys F., Fernandes V. and Caubit C. Prediction of relative permeability and fast wettability assessment using Digital Rock Physics: An operational study on a Reservoir Sandstone. SCA2023-26, (2023).
3. W.G. Anderson, “Wettability literature survey-part 5: The effects of wettability on relative permeability,” J Pet Technol 39, 1453. (1987).
4. McDougall, S.R., Sorbie, K.S.: The Impact of wettability on Waterflooding: Pore-Scale Simulation. SPE-25271-PA 10(03), 208–213, (1995).
5. Sorbie KS, Skauge A. Can Network Modeling Predict Two-Phase Flow Functions? SPWLA-2012-v53n6a2 2012;53(06):401–9, (2012).
6. Bondino I, Hamon G, Kallel W, Kac D. Relative Permeabilities From Simulation in 3D Rock Models and Equivalent Pore Networks: Critical Review and Way Forward1. SPWLA-2012-v53n6a2 2013;54(06):538–46, (2013).

7. Garfi G., John C.M., Rücker M., Lin Q., Spurin C., Berg S. and Krevor S. Determination of the spatial distribution of wetting in the pore networks of rocks, J Colloid Interface Sci., 613, 786, (2022).
8. M. Rücker, W.-B. Bartels, K. Singh, N. Brussee, A. Coorn, H. Van Der Linde, A. Bonnin, H. Ott, S. Hassanizadeh, M. Blunt et al., The effect of mixed wettability on pore-scale flow regimes based on a flooding experiment in ketton limestone, Geophys. Res. Lett. 46, 3225, (2019).
9. T. Akai, A. M. Alhammadi, M. J. Blunt, and B. Bijeljic, Modeling oil recovery in mixed-wet rocks: Pore-scale comparison between experiment and simulation, Trans. Porous Med. 127, 393, (2019).
10. Foroughi S, Bijeljic B, Lin Q, Raeini AQ, Blunt MJ. Pore-by-pore modeling, analysis, and prediction of two-phase flow in mixed-wet rocks. Phys. Rev. E, 102(2):23302, (2020).
11. Alhammadi, A. M., AlRatrout, A., Singh, K., Bijeljic, B. & Blunt, M. J. In situ characterization of mixed-wettability in a reservoir rock at subsurface conditions. Sci. Rep. 7, 10753, (2017).
12. AlRatrout, A., Raeini, A.Q., Bijeljic, B., Blunt, M.J.: Automatic measurement of contact angle in pore-space images. Advances in Water Resources 109, 158–169, (2017).
13. Andrew, M., Bijeljic, B., Blunt, M.J.: Pore-scale contact angle measurements at reservoir conditions using X-ray microtomography. Advances in Water Resources 68, 24–31, (2014)
14. AlRatrout A, Blunt MJ, Bijeljic B. Spatial Correlation of Contact Angle and Curvature in Pore-Space Images. Water Resour. Res., 54(9):6133–52, (2018).
15. Sun C., McClure J.., Mostaghimi P., Herring A.L., Meisenheimer D.E., Wildenschild D., Berg S., Armstrong R.T. Characterization of wetting using topological principles. J Colloid Interface Sci., 578:106–15, (2020).
16. Regaieg M., Bondino I., Varloteaux C, Farhana Faisal T., Yang J. and Rivenq R. Large two phase Digital Rock Physics simulations for relative permeability uncertainty assessment. SCA2021-007, (2021).
17. Q. Lin, Y. Al-khulaifi, B. Bijeljic and M.J. Blunt, 'Quantification of sub-resolution porosity in carbonate rocks by applying high-salinity contrast brine using Xray microtomography differential imaging', Advances in Water Resources. 96, (2016).
18. Yang J, Bondino I, Regaieg M, Moncorgé A. Pore to pore validation of pore network modelling against micromodel experiment results. Computational Geosciences, 21(5):849–62, (2017).
19. Saxena N, Hofmann R, Alpak FO, Dietderich J, Hunter S, Day-Stirrat RJ. Effect of image segmentation & voxel size on micro-CT computed effective transport & elastic properties. Marine and Petroleum Geology, 86:972–90, (2017).
20. Wang X, Yu K, Wu S, Gu J, Liu Y, Dong C, Qiao Y, Change Loy C. Esrgan: Enhanced super-resolution generative adversarial networks. In: Proceedings of the European conference on computer vision (ECCV) workshops. p. 0.
21. Regaieg M, Varloteaux C, Farhana Faisal T, ElAbid Z. Towards Large-Scale DRP Simulations: Generation of Large Super-Resolution images and Extraction of Large Pore Network Models. Transport in Porous Media, 147(2):375–99, (2023).
22. Arganda-Carreras I, Kaynig V, Rueden C, Eliceiri KW, Schindelin J, Cardona A, Sebastian Seung H. Trainable Weka Segmentation: a machine learning tool for microscopy pixel classification. Bioinformatics, 33(15):2424–6, (2017).
23. Berg S, Saxena N, Shaik M, Pradhan C. Generation of ground truth images to validate micro-CT image-processing pipelines. The Leading Edge, 37(6):412–20, (2018).
24. Reinhardt M, Jacob A, Sadeghnejad S, Cappuccio F, Arnold P, Frank S, Enzmann F, Kersten M. Benchmarking conventional and machine learning segmentation techniques for digital rock physics analysis of fractured rocks. Environmental Earth Sciences, 81(3):71, (2022).
25. Raeini AQ, Bijeljic B, Blunt MJ. Generalized network modeling: Network extraction as a coarse-scale discretization of the void space of porous media. Phys. Rev. E. 96(1):13312, (2017).
26. Pairoys, F., Caubit, C., Rochereau, L., Nepesov, A., Danielczick, Q., Agenet, N., Nono, F.; Impact of Dopants on SCAL Experiments, Phase I; SCA2023-007, (2023).
27. Nono F., Farhana Faisal, T., Fischer F., Pairoys F., Regaieg M., and Caubit C; Pore scale investigation of dopants impact on wettability alteration; SCA2024-1025, (submitted).
28. Fernandes, V., Nono, F., Nicot, B., Pairoys, F., Bertin, H., Lachaud, J., and Caubit, C.; Hybrid Drainage Technique application on bimodal limestone; SCA2023-006, (2023).
29. Dixit AB, Buckley JS, McDougall SR, Sorbie KS. Empirical measures of wettability in porous media and the relationship between them derived from pore-scale modelling. Transport in Porous Media, 40(1):27–54, (2000).
30. Regaieg M, Moncorgé A. Adaptive dynamic/quasi-static pore network model for efficient multiphase flow simulation. Computational Geosciences, 21(4):795–806, (2017).
31. Sergent M. Contribution de la Méthodologie de la Recherche Expérimentale à l'élaboration de matrices uniformes: Application aux effets de solvants et de substituants. Aix-Marseille 3, (1989).